AFRL-RV-PS-
TR-2014-0104

UNDERSTANDING THE BALANCE OF DAYSIDE AND NIGHTSIDE RECONNECTION CONTRIBUTIONS TO THE CROSS POLAR CAP POTENTIAL DURING SOLAR WIND DISTURBANCES

Christos Christodoulou

University of New Mexico
1 University of New Mexico
Albuquerque, NM 87131-0001

15 May 2014

Final Report

AIR FORCE RESEARCH LABORATORY
Space Vehicles Directorate
3550 Aberdeen Ave SE
AIR FORCE MATERIEL COMMAND
KIRTLAND AIR FORCE BASE, NM 87117-5776

DTIC COPY

NOTICE AND SIGNATURE PAGE

Using Government drawings, specifications, or other data included in this document for any purpose other than Government procurement does not in any way obligate the U.S. Government. The fact that the Government formulated or supplied the drawings, specifications, or other data does not license the holder or any other person or corporation; or convey any rights or permission to manufacture, use, or sell any patented invention that may relate to them.

This report was cleared for public release by the 377 ABW Public Affairs Office and is available to the general public, including foreign nationals. Copies may be obtained from the Defense Technical Information Center (DTIC) (http://www.dtic.mil).

AFRL-RV-PS-TR-2014-0104 HAS BEEN REVIEWED AND IS APPROVED FOR PUBLICATION IN ACCORDANCE WITH ASSIGNED DISTRIBUTION STATEMENT.

//SIGNED//	//SIGNED//
Dr. Daniel Ober	Edward J. Masterson, Colonel, USAF
Program Manager/RVBXP	Chief, Battlespace Environment Division

This report is published in the interest of scientific and technical information exchange, and its publication does not constitute the Government's approval or disapproval of its ideas or findings.

REPORT DOCUMENTATION PAGE

Form Approved
OMB No. 0704-0188

1. REPORT DATE *(DD-MM-YYYY)*	**2. REPORT TYPE**	**3. DATES COVERED** *(From - To)*
15-05-2014	Final Report	28 Nov 12 to 30 Nov 13

4. TITLE AND SUBTITLE
Understanding the Balance of Dayside and Nightside Reconnection Contributions to the Cross Polar Cap Potential During Solar Wind Disturbances

5a. CONTRACT NUMBER
FA9453-13-1-0231

5b. GRANT NUMBER

5c. PROGRAM ELEMENT NUMBER
61102F

6. AUTHOR(S)
Christos Christodoulou

5d. PROJECT NUMBER
3001

5e. TASK NUMBER
PPM00016116

5f. WORK UNIT NUMBER

7. PERFORMING ORGANIZATION NAME(S) AND ADDRESS(ES)
University of New Mexico
1 University of New Mexico
Albuquerque, NM 87131-0001

8. PERFORMING ORGANIZATION REPORT NUMBER

9. SPONSORING / MONITORING AGENCY NAME(S) AND ADDRESS(ES)
Air Force Research Laboratory
Space Vehicles Directorate
3550 Aberdeen Avenue SE
Kirtland AFB, NM 87117-5776

10. SPONSOR/MONITOR'S ACRONYM(S)
AFRL/RVBXP

11. SPONSOR/MONITOR'S REPORT NUMBER(S)
AFRL-RV-PS-TR-2014-0104

12. DISTRIBUTION / AVAILABILITY STATEMENT
Approved for public release; distribution is unlimited. (377ABW-2014-0431 dtd 10 Jun 2014)

13. SUPPLEMENTARY NOTES

14. ABSTRACT

This study focused on the investigation of how solar wind energy is deposited into the magnetosphere-ionosphere system during sudden enhancements of solar wind dynamic pressure (Psw), using the coupled OpenGGCM-CTIM 3D global magnetosphere – ionosphere – thermosphere model. Three unique events of solar wind pressure enhancements that occurred during negative, near-zero, and positive IMF Bz were simulated. Then, the behavior of the dayside and nightside reconnection rates were examined, and their respective contributions to Cross Polar Cap Potential (CPCP), a proxy of ionospheric plasma convection strength, were quantified. The modeled CPCP increased after a Psw enhancement in all three cases, which agrees well with observations from the Defense Meteorological Satellite Program (DMSP) spacecraft and predictions from the Assimilative Mapping of Ionospheric Electrodynamics (AMIE) technique. In the OpenGGCM-CTIM model, dayside reconnection increased within 9-13 minutes of the pressure impact, while nightside reconnection intensified about 13-25 minutes after the pressure increase. As the strong Psw compresses the dayside magnetosheath and, subsequently, the magnetotail, their magnetic fields intensify and activate stronger anti-parallel reconnection on the dayside magnetopause first and near the central plasma sheet second. For southward IMF, dayside reconnection contributes to the CPCP enhancement two to four times more than nightside reconnection. For northward IMF, the dayside contribution weakens, and nightside reconnection contributes more to the CPCP enhancement. It was found that high-latitude magnetopause reconnection during northward IMF produced sunward ionospheric plasma convection, which decreases the typical dawn-to-dusk ionosphere electric field. This results in a weaker dayside reconnection contribution to the CPCP during northward IMF.

15. SUBJECT TERMS
reconnection contributions, solar wind energy, dayside and nightside reconnection, ionospheric electrodynamics

16. SECURITY CLASSIFICATION OF:			**17. LIMITATION OF ABSTRACT**	**18. NUMBER OF PAGES**	**19a. NAME OF RESPONSIBLE PERSON**
a. REPORT	**b. ABSTRACT**	**c. THIS PAGE**			Dr. Daniel Ober
Unclassified	Unclassified	Unclassified	Unlimited	40	**19b. TELEPHONE NUMBER** *(include area code)*

This page is intentionally left blank.

TABLE OF CONTENTS

LIST OF FIGURES

ABSTRACT

This study focused on the investigation of how solar wind energy is deposited into the magnetosphere-ionosphere system during sudden enhancements of solar wind dynamic pressure (P_{sw}), using the coupled OpenGGCM-CTIM 3D global magnetosphere – ionosphere – thermosphere model. Three unique events of solar wind pressure enhancements that occurred during negative, near-zero, and positive IMF B_z were simulated. Then, the behavior of the dayside and nightside reconnection rates were examined, and their respective contributions to Cross Polar Cap Potential (CPCP), a proxy of ionospheric plasma convection strength, were quantified. The modeled CPCP increased after a P_{sw} enhancement in all three cases, which agrees well with observations from the Defense Meteorological Satellite Program (DMSP) spacecraft and predictions from the Assimilative Mapping of Ionospheric Electrodynamics (AMIE) technique. In the OpenGGCM-CTIM model, dayside reconnection increased within 9-13 minutes of the pressure impact, while nightside reconnection intensified about 13-25 minutes after the pressure increase. As the strong P_{sw} compresses the dayside magnetosheath and, subsequently, the magnetotail, their magnetic fields intensify and activate stronger anti-parallel reconnection on the dayside magnetopause first and near the central plasma sheet second. For southward IMF, dayside reconnection contributes to the CPCP enhancement two to four times more than nightside reconnection. For northward IMF, the dayside contribution weakens, and nightside reconnection contributes more to the CPCP enhancement. It was found that high-latitude magnetopause reconnection during northward IMF produced sunward ionospheric plasma convection, which decreases the typical dawn-to-dusk ionosphere electric field. This results in a weaker dayside reconnection contribution to the CPCP during northward IMF.

1. INTRODUCTION

Recent studies have established that sudden enhancements of solar wind dynamic pressure (P_{sw}) result in intense magnetosphere-ionosphere interactions, indicating that P_{sw} enhancements can be a significant driver to transport solar wind energy into the magnetosphere-ionosphere (MI) system. The MI responses to strong solar wind pressure include auroral oval expansion [Lyons, 2000; Zesta et al., 2000; Boudouridis et al., 2003, 2005], polar cap area reduction [Boudouridis et al., 2003, 2004b, 2005], enhanced transpolar potential [Boudouridis et al., 2004a, 2008b; Ober et al., 2006, 2007] and fast ionospheric plasma convection [Boudouridis et al., 2007, 2008a, 2011].

It has been inferred that during periods of strong solar wind pressure, magnetic reconnection intensifies in both the dayside and the nightside magnetosphere. Boudouridis et al. [2007, 2011] analyzed the ionospheric convection patterns using Super Dual Auroral Radar Network (SuperDARN) observations, and showed that the dayside ionospheric flow velocities in the vicinity of the expected dayside open-closed boundary (separatrix) location significantly increase within four minutes of the sudden enhancement of solar wind pressure, indicating strong magnetopause reconnection after the pressure impact. In addition, Boudouridis et al. [2011] observed a significant increase of the nightside ionospheric flow velocities 10–15 minutes after the P_{sw} impact, which implies intense nightside reconnection. Particle precipitation data from the Defense Meteorological Satellite Program (DMSP) and auroral images from the Polar Ultra Violet Imager (UVI) [Lyons, 2000; Zesta et al., 2000; Milan et al., 2004b; Hubert et al., 2006b, 2009; Boudouridis et al. 2003, 2004b, 2008a] show that the high-latitude auroral oval boundary moves poleward across the nightside region during strong solar wind pressure enhancements. This open flux reduction on the nightside magnetosphere is a direct indication of magnetotail reconnection enhancement.

Although previous studies have provided evidence of intensification of dayside and nightside reconnection, the following fundamental questions are still unanswered: (1) how the reconnection rates vary throughout the P_{sw} enhancement, (2) which physical process causes the reconnection rate increase, and (3) how strongly they contribute to the ionospheric convection enhancement that is simultaneously observed. Due to poor data coverage of satellite and ground observations throughout the entire MI system, these questions cannot be solved solely by

observations. This research work addressed these open questions using the three-dimensional global magnetosphere–ionosphere–thermosphere model, the Open Geospace General Circulation Model – Coupled Ionosphere Thermosphere Model (OpenGGCM-CTIM).

The magnetosphere-ionosphere responses to three P_{sw} enhancement events that occurred during negative, near-zero, and positive IMF B_z were simulated. Zesta et al. [2000] and Boudouridis et al. [2003; 2011] have investigated these events using ground magnetometer, DMSP, SuperDARN, and Polar UVI observations. We compared such observations with our model simulations of these events. The model-data comparison was conducted in a qualitative way to test whether the simulations follow general trends of the observations. Once a good agreement of the simulation results with key observations was achieved, the full 3D global model results were used to investigate reconnection patterns in the dayside and nightside magnetosphere and quantify their relative importance to ionospheric convection. The simulations compensate for the limited coverage of observations and provide insight into the physical cause of observed MI coupling effects.

2. METHODOLOGY

2.1 OpenGGCM-CTIM model

OpenGGCM-CTIM is a three-dimensional coupled magnetosphere–ionosphere–thermosphere model. It divides the Earth's geospace system into three regions, the magnetosphere, the MI coupling zone, and the ionosphere-thermosphere system, and applies different calculation strategies based on the main physical process of each region.

OpenGGCM calculates plasma behavior in the outer magnetosphere by solving resistive MHD equations as an initial-boundary-value problem. The inner boundary of the magnetosphere is located at 3–4 R_E from the center of the Earth, and its outer boundary extends to the OpenGGCM simulation box. The X range of the simulation box extends from 20–30 R_E sunward to 600–2000 R_E anti-sunward, and its Y/Z range is from -48 to +48 R_E. The simulation box is spacious enough to cover the whole magnetosphere and its surrounding environments such as bow shock and magnetosheath. In particular, the size of the simulation domain ensures super-magnetosonic velocities on all outer boundaries. This ensures that all flow characteristics are

either inward (on the sunward side) or outward (on all other sides) so that the boundaries create no unwanted perturbations. The numerical grids are non-uniform Cartesian grids with small grid spacing (~0.1-0.2 R_E) near the dayside magnetosphere and near $Y_{gse}=Z_{gse}=0$, where magnetic reconnection is expected to occur. OpenGGCM uses solar wind conditions from ACE, WIND, or Geotail spacecraft as input, and provides number density, velocity, plasma pressure, and electromagnetic fields as output.

The MI coupling regime extends from the ionosphere to the inner boundary of the MHD calculation, at ~3.5 R_E from the Earth center. In this region the MHD equations are not solved, but relevant quantities such as field aligned currents (FAC) and the electric potential are mapped back and forth between the magnetosphere and the ionosphere. Also, electron precipitation parameters are computed from magnetosphere parameters and mapped to the ionosphere, where they are used in CTIM. The OpenGGCM assumes a two-dimensional electrodynamic ionosphere and uses an ionospheric potential equation as a function of Field Aligned Currents (FACs) and ionospheric conductance by assuming that the FACs generated from the solar wind–magnetosphere interaction should be closed in the ionosphere [Raeder et al., 1998, 2001; Raeder, 2003]. To calculate the electric potential, OpenGGCM obtains FACs from the inner boundary of the magnetosphere, and maps them to the ionosphere along the dipole magnetic field lines. Ionospheric conductance is obtained from CTIM, which is a three-dimensional dynamic model of the ionosphere-thermosphere system that self-consistently solves both neutral and ion fluid equations from 80 km to several 1000 km in altitude, providing realistic ionospheric conductance to OpenGGCM. Finally, the OpenGGCM maps the obtained electric potentials back to the inner boundary of the magnetosphere, and uses them to provide the magnetospheric plasma flow boundary conditions on that boundary, closing the electrodynamic MI coupling cycle originally developed by Vasyliunas [1970] and Wolf et al. [1975, 1983]. More detailed information about the OpenGGCM and CTIM models can be found in Raeder et al. [2001, 2003, 2008] and Fuller-Rowell et al. [1996].

2.2 Calculation of reconnection rates

Under the assumption of a quasi-static magnetosphere, the dayside and nightside reconnection rates (Φ_D and Φ_N) are given by the integral of $E \cdot dl$ along the dayside and nightside Open-Closed field line Boundary (OCB), where electric field $\boldsymbol{E}$ is $(V_b - V_p) \times B$ and $d\boldsymbol{l}$

is an infinitesimal distance along OCB. $\boldsymbol{V_b}$ and $\boldsymbol{V_p}$ are the normal velocity of the OCB and the velocity of the ionospheric plasma flow perpendicular to the OCB, respectively. Thus,

$$\Phi=\int (V_b - V_p)\times B\cdot dl \,. \quad (1)$$

The term $V_b - V_p$ indicates the ionospheric flow in the OCB moving frame of reference. $E=(V_b - V_p)\times B$ is therefore the ionospheric electric field in the OCB moving frame of reference which should be equal to the electric field at the distant merging site assuming no field aligned potential drops and no inductive electric fields. If the OCB is stationary (i.e. $V_b = 0$) then the reconnection rate is equivalent to the electrostatic potential along the OCB. This calculation method is adopted from previous observational and theoretical studies on merging rates [de La Beaujardiere et al., 1991; Blanchard et al., 1996; Ober et al., 2001, 2007; Hubert et al, 2006a].

To obtain the open-closed field line boundary, the magnetic field lines from every ionospheric grid point through the magnetosphere were traced. The ionosphere grid resolution was 3°× 0.5° in magnetic longitude and latitude, respectively. The tracing was stopped when the field line returned to the inner boundary of the magnetosphere, when it reached the outer boundary of the simulation box, or when its length exceeds 1,000 R_E. If a field line reached the inner boundary, it was considered to be as a closed field line; otherwise, it was assumed to be an open field line. The ionospheric grids connected to closed and open field lines were marked with -1 and 1, respectively. The zero contour of those grids is the OCB. To determine the dayside and nightside open-closed field line boundary, the ionospheric electric potentials were calculated along the OCB from the OpenGGCM-CTIM results and selected the locations of maximum and minimum potentials which appeared at the dawn and dusk sectors, respectively. The dayside OCB was the region from maximum to minimum potentials that crossed the dayside ionosphere, and the nightside OCB was the remainder.

In order to obtain the dayside reconnection rate, c the first term of the reconnection rate integral, $\int V_b \times B\cdot dl$, was calculated by measuring the open flux per unit time crossing the dayside open closed field line boundary and the second term, $-\int V_p \times B\cdot dl$, by obtaining the electric potential difference along the dayside OCB. The same procedure was applied for the calculation of nightside reconnection rate except that the two nightside integrals were measured along the nightside OCB. No potential drop along the magnetic field lines was assumed. Under this assumption, the electric potential across magnetospheric reconnection lines was projected to

the ionosphere. However, the numerical model solves the MHD equations on a grid, such that the discretization may introduce non-physical parallel electric fields along the field lines. Due to this numerical artifact, the reconnection rates calculated from ionospheric variables may not exactly match the reconnection rates in the magnetosphere. The numerically induced potential drop ranged a few kV to ~10 kV in the model, while the reconnection rate varied from several tens to hundreds of kV. Thus, the potential drop between the reconnection line and the ionosphere was minimal, compared to the reconnection rate, and therefore any mismatch between the magnetospheric and ionospheric electric potentials could be neglected for the purpose of this study.

2.3 The relation between reconnection rates and CPCP

This work investigated the balance of dayside and nightside reconnection rates and their relative contribution to a dramatic increase of ionospheric flows that occurs immediately following a sharp magnetospheric compression. To explain such a relation, the cross polar cap potential (CPCP) as a proxy of the ionospheric convection strength was adopted, and fitted the model results to the CPCP equation of the Expanding and Contracting Polar Cap (ECPC) model [Lockwood, 1991; Lockwood and Cowley 1992]:

$$\Phi_{\mathrm{CPCP}} = \mathrm{C}_D \Phi_D + \mathrm{C}_N \Phi_N + \Phi_V \qquad (2)$$

where Φ_{CPCP} is a transpolar potential, Φ_V is the viscous-like potential, and Φ_D (Φ_N) is the electric voltage caused by dayside (nightside) reconnection. C_D and C_N are regression coefficients of the dayside and nightside merging rate, respectively. These coefficients have been considered as weight factors that quantify the relative contribution of merging rates on the CPCP enhancement [Lockwood et al., 2009; Gordeev et al., 2011]. Note that in steady-state, when the dayside and nightside OCB motion is zero, $\Phi_D = \Phi_N = \Phi_{\mathrm{CPCP}} - \Phi_V$ and then the regression coefficients are $C_D = \mathrm{C}_N = 0.5$. Therefore, any difference of the coefficients from 0.5 could be interpreted to indicate departures from steady-state and then they would also represent the relative contributions of the two reconnection rates to the CPCP.

This work defined the CPCP to be the difference between the maximum and minimum ionospheric potentials. CPCP was produced by the combined effect of reconnection and viscous interaction. Assuming that the potential difference along the OCB (ΔP_{OCB}) is driven by magnetic

reconnection, the viscous-like potential (Φ_V) becomes $\Phi_v = \mathrm{CPCP} - \Delta \mathrm{P}_{\mathrm{OCB}}$. A multiple linear regression was used to fit the model results of reconnection rates and viscous potential to the above CPCP equation, and to obtain the regression coefficients that give the best fit results.

3. CASE STUDIES

3.1 Event 1: 10 January 1998

The first event occurred during the recovery phase of a geomagnetic storm on January 10, 1997. The top four panels of Figure 1 show IMF, solar wind speed, number density, and dynamic pressure obtained from the OMNI data during this event. The solar wind pressure increases from 2 to 6 nPa for 20 minutes while IMF stays southward. The vertical thick black line represents the arrival of a strong pressure front at the nose of the magnetopause. Previous studies of this event [Lyons, 2000; Zesta et al., 2000; Boudouridis et al., 2003; Boudouridis et al., 2005] have shown auroral oval expansion, polar cap closure, and enhanced CPCP.

The OpenGGCM-CTIM model simulated the magnetosphere–ionosphere responses to this event using solar wind parameters as input. Figure 1.e shows the polar cap area obtained from our model. After a few minutes of slight expansion near 11:00 UT, the modeled polar cap area continuously shrinks until 11:27 UT. Polar UVI Imager [Zesta et al., 2000] and DMSP SSJ/4 instruments [Boudouridis et al., 2003] also observe the polar cap closure after the pressure impact, agreeing with our model results.

Figure 1.f displays the cross-polar-cap potentials obtained by OpenGGCM-CTIM (blue line), Assimilative Mapping of Ionospheric Electrodynamics (AMIE) technique (green line) and DMSP spacecraft (red dots). The red horizontal lines represent the time periods for the spacecraft to estimate each CPCP value. DMSP satellites obtain a transpolar potential by integrating measured electric fields along the satellite trajectory that crosses the entire polar region. Thus, they provide an averaged picture of the CPCP and may miscalculate its magnitude if the DMSP orbit misses the center of the ionospheric potential pattern.

To compensate for this limitation, AMIE predictions of transpolar potential were used as additional data source for model-data comparison. The AMIE technique estimates the entire ionospheric electrodynamics, such as electric potentials, conductances, and currents, by

assimilating the observations from radar, ground magnetometer, and low-orbiting satellites. During intervals of good data coverage, AMIE provides reasonable electric field maps with an uncertainty of ~30% [Knipp and Emery, 1997]. The AMIE data presented in this study were calculated from 115 ~ 135 ground magnetometers and downloaded from http://vmr.engin.umich.edu/Model/_amie/.

Both, the DMSP and AMIE data were used to understand the general trend of CPCP and to test our model results. In Figure 1.f, DMSP data showed CPCP enhancement from 120 to 220 kV after the pressure impact, while AMIE shows a similar CPCP response although its magnitude is lower than the DMSP data. The model also showed a CPCP increase from 140 to 200 kV after the pressure change. Although the CPCP magnitudes were different, all the DMSP, AMIE, and OpenGGCM-CTIM data consistently and clearly show the enhancement of the transpolar potential after the pressure impact.

Difference of CPCP values from different data sources have been noticed in the previous studies. Kihn et al. [2006] showed that AMIE produces higher transpolar potentials than DMSP spacecraft if ground magnetometer data are used as the only input for AMIE. Slinker et al. [1999] and Raeder [2005] found that MHD models tend to predict higher CPCP than AMIE. In spite of the difference in CPCP magnitude, these studies showed a reasonable correlation between the DMSP and AMIE data and between the AMIE and MHD data, supporting that our qualitative model-data comparison with these CPCP data are reliable.

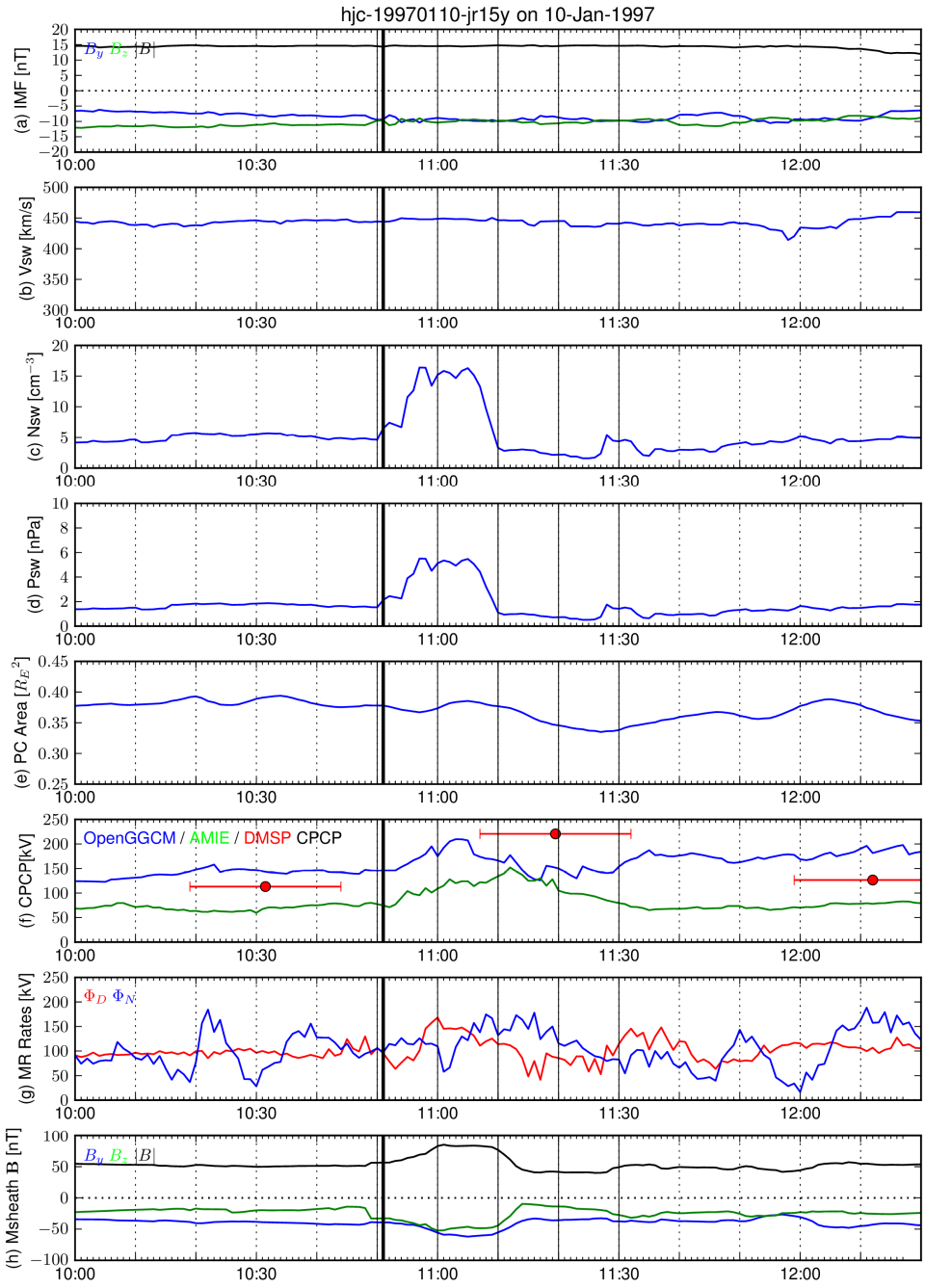

Figure 1. The OMNI solar wind data (a-d) and the OpenGGCM-CTIM results (e-h) on January 10, 1997. *The top four panels show IMF, solar wind plasma speed (V_{sw}), number density (N_{sw}), and dynamic pressure (P_{sw}). The bottom four panels represent the polar cap area, cross polar cap potential, reconnection rates, and magnetosheath magnetic fields obtained from the OpenGGCM-CTIM model. The red dots and horizontal lines in Figure 1.f represent DMSP transpolar potentials and the observation periods for the satellites to measure each CPCP. The blue and green lines in Figure 1.f show the cross-polar-cap potentials predicted from OpenGGCM-CTIM and AMIE. The red and blue lines in Figure 1.g are the reconnection rates of dayside and nightside magnetosphere, respectively. The thick vertical lines indicate when the P_{sw} enhancement arrives at the nose of the magnetopause, and the thin vertical lines represent the times selected for the magnetosphere plots. All magnetic field vectors are in the GSE coordinate system.*

Figure 1.g shows the reconnection rates of OpenGGCM-CTIM. These rates were calculated based on the method presented in section 2.2. The dayside reconnection rate (Φ_D) reacts first to the P_{sw} enhancement, increasing from 60 to 160 kV within a few minutes after the pressure change. The polar cap expands near ~11:00 UT due to the enhanced dayside reconnection rate (see Figure 1.e). The nightside reconnection rate (Φ_N) reached its maximum value at 11:09 UT, ~9 minutes later than the dayside reconnection rate. The magnetotail reconnection became stronger than the magnetopause reconnection during 11:05 ~ 11:27 UT. As a result, the polar cap area decreased continuously until the next, relatively weak pressure enhancement hit the dayside magnetosphere at 11:27 UT.

To understand why magnetopause reconnection intensifies during a P_{sw} enhancement, the magnetic fields of the magnetosheath in Figure 1.h are displayed, which were obtained from the model results at 1 R_E sunward from the magnetopause nose. Although the IMF magnitude was steady during that time (black line in Figure 1.a), the total magnetic field of the magnetosheath (black line in Figure 1.h) jumped up to 85 nT in response to the solar wind pressure increase. The total magnetosheath field dropped quickly as the P_{sw} decreased at ~11:07 UT, and enhanced again as the P_{sw} slightly increased at 11:27 UT, so it varied in phase with P_{sw}. Thus, the sudden increase of solar wind dynamic pressure compressed the magnetosheath total magnetic field, which in turn increased the reconnection rate. This increase is analogous to the well-known pile-up reconnection first discussed by Parker [1973] and Sonnerup [1988]. As a result, stronger magnetosheath fields drape over the dayside magnetopause, activating more intense anti-parallel reconnection and thus increasing the dayside merging rate [see Dorelli et al., 2004].

Figure 2 displays the magnetosphere noon-midnight meridian plane during this event, and examines the dynamics of different variables. The dynamic pressure (P_{dy}), X component of velocity (V_x) in Geocentric Solar Ecliptic (GSE) coordinate system, total magnetic field ($|B|$), and X component of the magnetic field (B_x) in GSE coordinate system are plotted from left to right. We display the model output with a time resolution of 10 minutes from 10:50 to 11:30 UT as demonstrated from top to bottom of each column in Figure 2. The thin vertical lines in Figure 1 correspond to the timing of each column of Figure 2.

Figure 2.a and 2.b show the magnetosheath compression due to the sudden enhancement of the solar wind dynamic pressure. The nose of the bow shock moves from X_{gse} = 17 to 11 Re at

11:00 UT. This compression intensifies the total magnetic field of the magnetosheath and strengthens magnetopause reconnection. Figures 2.c and 2.d show the magnetosphere state when the solar wind pressure decreases to ~1 nPa, after the first compression, and when the bow shock location moves out to X_{gse} = 24 R_E at 11:20 UT. Because of the magnetosheath expansion, both the total magnetosheath field and dayside merging rate weaken at that time. The magnetosheath is compressed again at 11:30 UT when the smaller pressure enhancement arrives at the dayside magnetopause (See Figure 2.e). The bow shock moves back to X_{gse} = 22 R_E, which leads to the slight increase of the magnetosheath fields and of the dayside merging rate.

Figure 2.c, 2.d, and 2.e show that the sudden increase of solar wind pressure also affects the nightside magnetosphere. The pressure front reaches the near-Earth magnetotail (X_{gse} from -20 to -40 R_E) at 11:10 UT, and propagates to the distant tail (X_{gse} < -80 R_E) at 11:20 and 11:30 UT. As the pressure compresses the magnetotail, the magnetic field B_x near the central plasma sheet increases in both lobes. This leads to a stronger anti-parallel reconnection near X_{gse} = -30 R_E with faster earthward flows, as evidenced in the V_x panel. At 11:30 UT, the P_{sw} enhancement disappears to the very distant magnetotail. As a result, the near-Earth magnetotail expands and its magnetic field decreases. The earthward plasma speed also reduces to ~ 200 km/s, as a result of weaker nightside reconnection.

The compression by the P_{sw} enhancement intensifies magnetic fields of the magnetosheath and near the central plasma sheet, increasing dayside and nightside reconnection rates, respectively. Based on Figure 2.b and 2.c, the P_{sw} front takes about 10 minutes to move from the dayside to the nightside magnetosphere. This explains why the nightside reconnection responds to the pressure impact ~9 minutes later than the dayside reconnection. The polar cap area thus expands for a short time period after the pressure impact due to the enhancement of dayside merging rate, but it soon closes when the nightside reconnection rate becomes dominant.

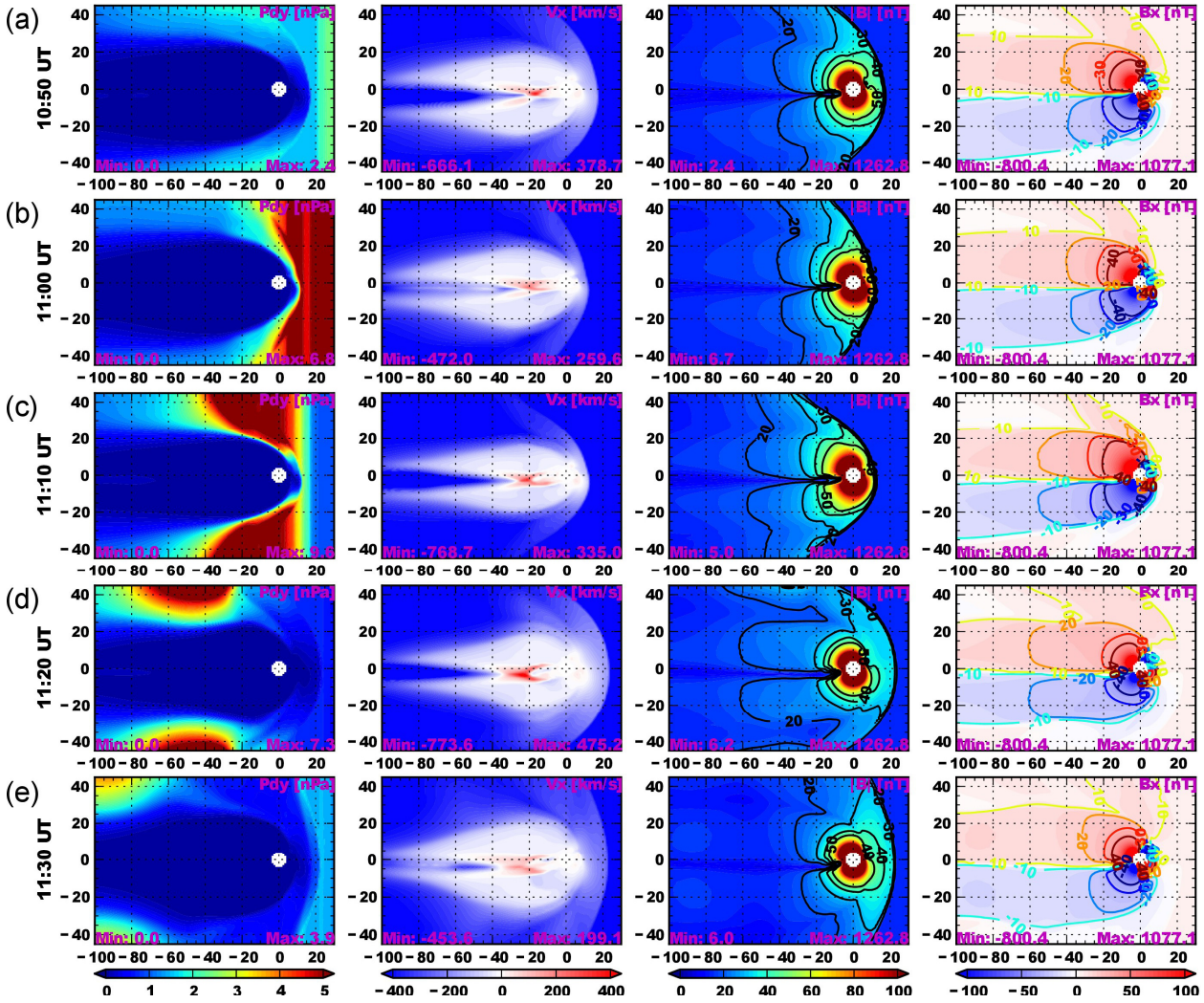

Figure 2. The OpenGGCM-CTIM magnetosphere plots during 10:50 – 11:30 UT on January 10, 1997. *Each column represents from left to right the dynamic pressure (P_{dy}), X_{gse} component of plasma velocity (V_x), total magnetic field ($|B|$), and X_{gse} component of magnetic field (B_x) on the noon-midnight meridian plane.*

3.2 Event 2: 30 April 1998

The second event occurred on April 30, 1998 during nearly zero IMF B_y and B_z. The top four panels of Figure 3 show IMF (in GSE coordinates), solar wind plasma speed, number density, and dynamic pressure observed by the WIND spacecraft. The solar wind data were time-shifted to account for the solar wind propagation from the WIND location to the nose of the magnetopause. At 09:25 UT, a shock impacted the magnetosphere. Solar wind number density and velocity abruptly increased, intensifying the solar wind dynamic pressure from 2 to 12 nPa. The IMF pointed southwest for the first 2 hours of the P_{sw} enhancement, and turned northeast after 11:30 UT. The major difference between this event and the previous one is that P_{sw}

remained increased for several hours during relatively weak IMF conditions, so it was a step change rather than a pulse.

The bottom four panels of Figure 3 show the polar cap area (area of open flux), transpolar potential, dayside and nightside reconnection rates, and magnetosheath fields calculated from the simulation of this event in the same format as in Figure 1. The blue line, green line, and red dots in Figure 3.f represent the time series of the CPCP calculated from the simulated data, AMIE, and DMSP observations, respectively. Similarly, the red horizontal lines in Figure 3.f represent the amount of time a full crossing of the auroral oval is completed by a DMSP satellite in order for a single value of CPCP to be calculated. As it was noted above, each single CPCP value represents an average of the transpolar potential for the time period indicated by the red lines.

The modeled polar cap expanded continuously during the first two hours of P_{sw} enhancement (Figure 3e). Most of this time, IMF was weakly southward (-2 to -3 nT in the solar wind and -10 to -20 nT in the magnetosheath). The total magnetosheath field intensified when the shock arrived, as expected. As a result, dayside reconnection significantly increased and the polar cap area opened. At 11:30 UT, the magnetosheath field turned northward. Dayside reconnection weakened, and nightside reconnection played a dominant role in the MI system, which lead to a polar cap closure.

Reduction of open flux area and polar cap size after the solar wind pressure enhancements has been observed in several studies [Zesta et al., 2000; Boudouridis et al., 2003, 2004b, 2005; Hubert et al., 2006b, 2009; Milan et al., 2009]. Depending on the IMF conditions, the closing happens only on the nightside and flank regions or over the whole Magnetic Local Time (MLT) locations including the dayside area [Boudouridis et al. 2003 and 2004b]. For this event, Boudouridis et al. [2004b] measured the poleward boundaries of auroral precipitation from a total of 16 DMSP satellite crossings over the pole region, and estimated the polar cap boundary motion after the P_{sw} impact. Due to the poor data coverage on the dayside ionosphere, they could not identify the dayside boundary motion, but observed that the nightside polar cap boundary moves poleward after the P_{sw} enhancement. This indicates closing of the nightside polar cap.

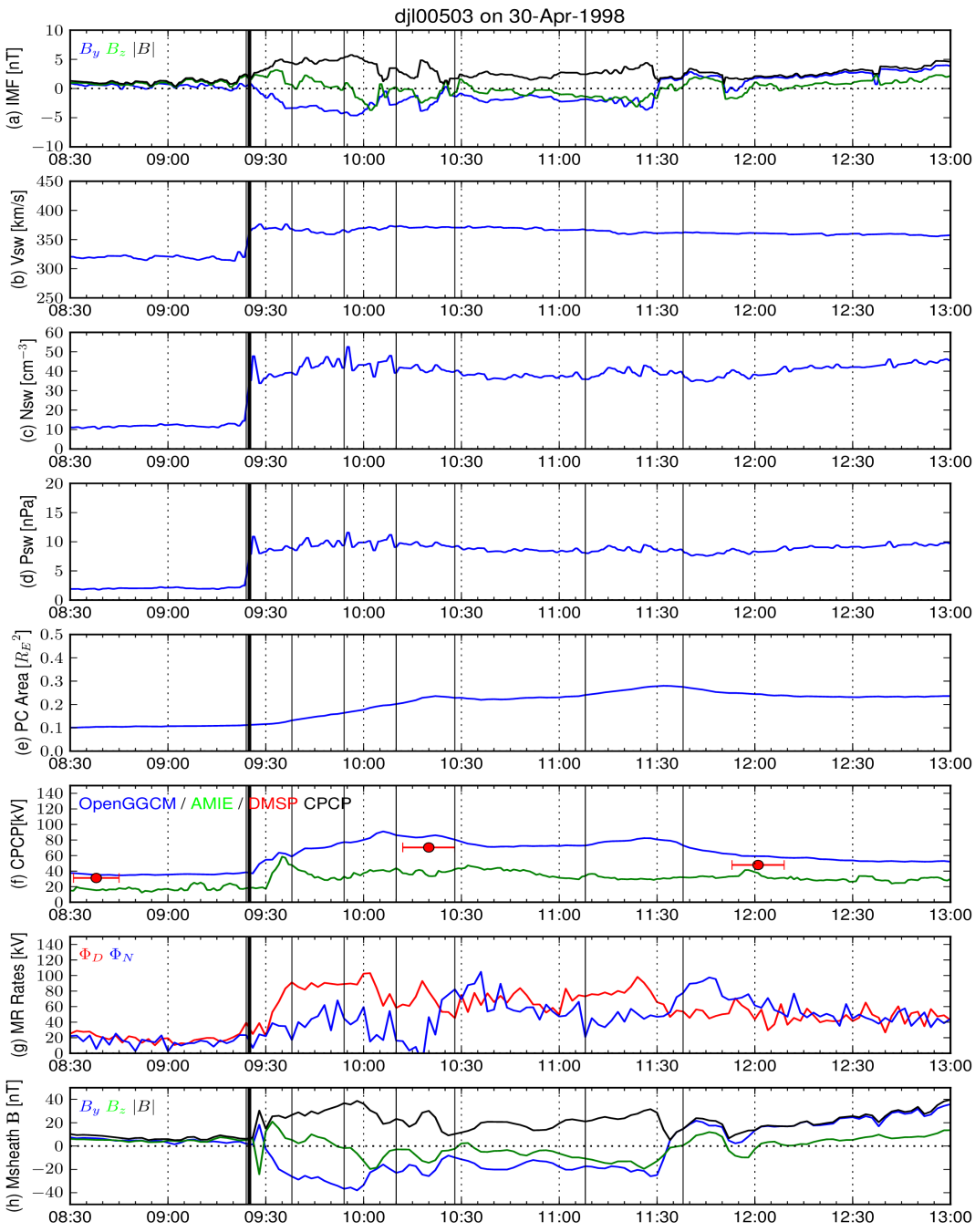

Figure 3. The WIND spacecraft measurements of solar wind conditions (a-d) and the OpenGGCM-CTIM results (e-h) on April 30, 1998. *The WIND data are time-shifted to account for the solar wind propagation from the satellite location to the magnetopause nose. See descriptions of Figure 1 for more details.*

The polar cap area is not a straightforward metric for the purpose of model-data comparison, due to the lack of complete MLT coverage of observations at the OCB, and the non-smooth OCB produced by the model simulations. Boudouridis et al. [2004b], for this same event, estimated the poleward boundary based on only a few data points observed at different times between 09:40–11:25 UT. Our model simulations produced very complicated polar cap boundaries during this observation period. Although the one-to-one comparison is difficult, our model showed an increase of the nightside reconnection rate during 9:25–9:50 UT and 10:20–10:45 UT (see Figure 3g). This indicates that the polar cap closes, at least on the nightside, twice in our model during the DMSP observation time. Hence, while our model indicated overall opening of the polar cap area, it did capture correctly some of the observational elements, and more than likely the balance between dayside and nightside reconnection rates may be different in the simulation environment than in the actual observations.

Unlike the motion of polar cap boundary, the CPCP showed excellent agreement between the model output and DMSP observations (see a blue line and red dots in Figure 3.f), demonstrating that our simulation provides a realistic response of ionospheric convection. The modeled CPCP increased to ~90 kV at 10:05 UT, after the compression, and then slowly decreased to ~50 kV for the next several hours, even though the solar wind dynamic pressure remained at high levels. DMSP observations showed similar CPCP increase from 35 to 70 kV at 10:20 UT and its subsequent decrease to 50 kV at 12:00 UT. Although predicting lower CPCP values than DMSP, AMIE produced a qualitatively similar CPCP response and confirmed that the DMSP transpolar potentials were reliable.

Figure 3.g shows the reconnection rates of OpenGGCM-CTIM. The dayside reconnection rate increased from 20 to 90 kV within 10 minutes after the P_{sw} increase. After this sudden rise, the rate slowly decreased for the next three hours. Unlike the first event, this was a shock, so the sharp solar wind dynamic pressure jump was accompanied by a similar increase in the IMF magnitude. Both of those contribute to a significant magnetopause reconnection increase, although we were not able to identify which parameter (P_{sw} or IMF) contributes more to the enhancement of dayside reconnection.

The nightside merging rate showed a more complex response than in our previous event. After the pressure impact, it exhibited three consecutive enhancements with local maximum at 09:50, 10:40, and 11:45 UT, the first peak occurring ~15 minutes after the dayside reconnection

peak. To understand the nightside dynamics, snapshots of the modeled magnetosphere at 09:24, 09:38, 09:54, 10:10, 10:28, 11:08, and 11:38 UT were displayed from top to bottom in Figure 4. The timing of each snapshot is also shown as a thin vertical line in Figure 3. Each column of Figure 4 represents, from left to right: the dynamic pressure ($P_{dy}=\rho v^2$), plasma pressure ($P_p=nkT$), X_{gse} component of plasma velocity (V_x), and X_{gse} component of magnetic field (B_x) on the noon-midnight meridian plane.

The top three rows of Figure 4 show the magnetosphere before and right after the pressure impact. At 09:24 UT, the pressure front has not yet reached the dayside magnetopause. Our model observed magnetotail reconnection near X_{gse} = -18 R_E evidenced by the oppositely directed fast plasma flows there. At 09:38 UT, the pressure front moves to the near-Earth magnetotail. The fast earthward flow of the prior instance significantly reduced now, indicating that the previous nightside reconnection subsides. As the P_{sw} compressed the magnetotail at 09:38 UT, the central plasma sheet stretched out into the more distant tail, as evidenced by the intensification of plasma pressure along the X axis in Figure 4.b. At the same time, the magnetic field B_x increased in both the northern and southern magnetotail lobes. At 09:54 UT, the pressure front has reached the distant tail, thus a broader region of the nightside magnetosphere was being compressed and B_x near the central plasma sheet continued to increase. This initiated anti-parallel reconnection near X_{gse} = -27 R_E, creating again fast earthward plasma flows.

The bottom four rows of Figure 4 show the magnetosphere after the strong pressure has engulfed most of the magnetotail. At these times, the impact of solar wind pressure front disappeared and the nightside magnetosphere adjusted to the new high pressure level. The dayside merging rate stayed high until 11:30 UT and loaded solar wind field and plasma in the magnetotail lobes. As a result, our model observed a plasmoid structure near X_{gse} = -25 R_E at 10:10 UT, and a thick and dense plasma sheet at 11:08 UT (see the plasma pressure in the third columns of Figure 4.d and 4.f). When the magnetosheath field turned northward at the instances of 10:28 and 11:35 UT, the nightside reconnection dominated and sent the previously piled-up plasma back to the inner magnetosphere with strong earthward flows at 10:28 and 11:39 UT.

The magnetotail compression by the P_{sw} enhancement produced the first peak of the nightside reconnection rate at 09:50 UT. As the pressure maintained its strength for several hours, the magnetotail adjusted to the new pressure strength, repeating the loading-unloading process. This created the other nightside reconnection peaks at 10:28 and 11:35 UT, in Figure

3.g.

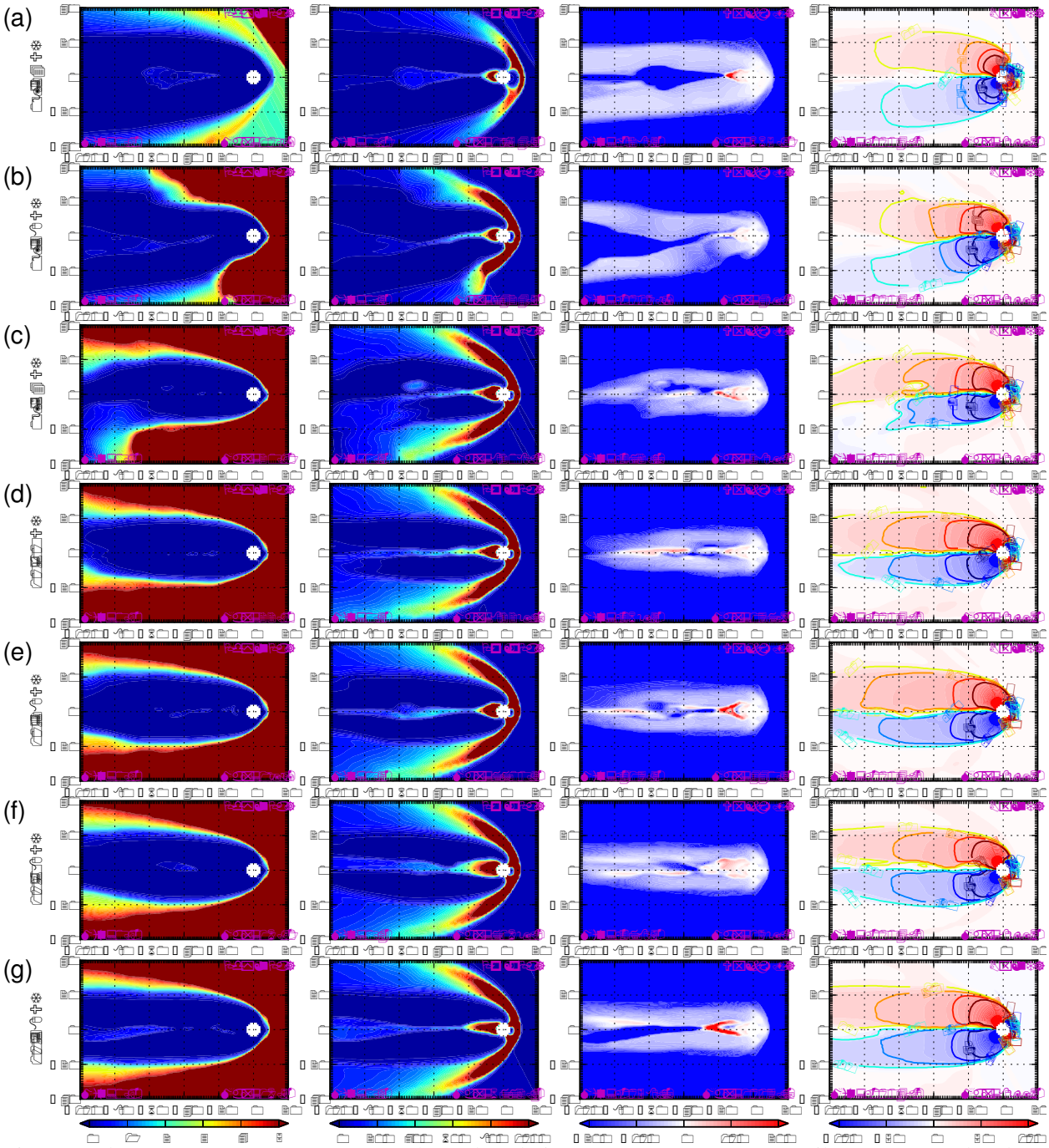

Figure 4. The OpenGGCM-CTIM magnetosphere plots during 09:24 – 11:38 UT on April 30, 1998. *Each column displays from left to right the dynamic pressure (P_{dy}), plasma pressure (P_p), X_{gse} component of plasma velocity (V_x), and X_{gse} component of magnetic fields (B_x) on the noon-midnight meridian plane. The times of each magnetosphere plot are marked as thin vertical lines in Figure 3.*

3.3 Event 3: 12 October 2000

The last event was a shock that occurred on October 12, 2000 during northward IMF. The top four panels of Figure 5 show the solar wind conditions observed by the Geotail spacecraft. At 22:29 UT, the solar wind pressure jumped from 1 to 6 nPa while the IMF magnitude increased from 5 to 15 nT. The enhanced P_{sw} and IMF were sustained for the next several hours, while the IMF B_z remained primarily northward with a strong positive B_y.

The bottom four panels of Figure 5 show the OpenGGCM-CTIM results. Due to the enhancements of solar wind pressure and IMF magnitude, the total magnetosheath field intensified. This lead to the increase of dayside reconnection rate and the opening of the polar cap area at ~ 22:37 UT. The nightside reconnection rate showed two local peaks at 22:42 and 23:11 UT. As this rate exceeded the dayside reconnection rate starting at ~22:45 UT, the polar cap area continuously shrinked. When the magnetosheath field turned slightly southward at 23:30 UT, the dayside reconnection abruptly increased and the polar cap area re-opened, as seen in Figure 5.e.

Figure 5.f shows the transpolar potentials obtained from the OpenGGCM-CTIM (blue line), AMIE (green line) and DMSP (red dots for the 3 available DMSP passes). The modeled CPCP jumped from 36 to 70 kV within a few minutes after the shock impact, and slowly increased for the remainder of this period. The DMSP spacecraft do not observe the CPCP increase during the pass centered at 23:02 UT because that orbit does not cross high-latitude ionosphere (the highest latitude of this orbit is 75.87° magnetic latitude, while others are at least over 79.84° magnetic latitude), thus missing the potential pattern peaks and severely underestimating the CPCP. Over the following orbit centered at 23:50 UT however, DMSP did record a significant increase in the CPCP, as that orbit crossed near the center of the potential pattern (the orbit reaches up to 79.84° magnetic latitude). Due to the poor DMSP data immediately after the compression, we focused on the AMIE data instead on a model-data comparison. Both AMIE and OpenGGCM-CTIM observed significant CPCP enhancement up to 70 kV at 22:32 UT, the increase lasting for many hours after the initial compression as the P_{sw} remained at high levels as well.

The reconnection patterns in Figure 5.g are also consistent with the responses of the ionospheric plasma flows. This event has been studied before by Boudouridis et al. [2011], who used the SuperDARN observations to show a dramatic enhancement of the dayside ionospheric

flows at ~22:35 UT, immediately after the compression. The reconnection patterns that we calculated and which are shown in Figure 5.g were consistent with the Boudouridis et al. [2011] observations. The dayside merging rate from our simulation in Figure 5.g increased at ~22:37 UT, just when Boudouridis et al. [2011] observed the dayside flow enhancement. The nightside reconnection rate from our simulation reached its first peak at 22:42 UT, and increases significantly around 23:10 UT in Figure 5.g. This is also in complete agreement with the Boudouridis et al. [2011] results, which observed the first enhancement of nightside flows at ~22:42 UT, and the spreading of the fast flow to a much broader region of the nightside ionosphere during 22:54 – 23:16 UT.

The dayside merging rate increases as the total magnetosheath field intensifies due to the combined effect of P_{sw} and IMF enhancements. Therefore, for this event, the dayside reconnection increase is not solely due to the P_{sw} enhancement. The nightside merging rate enhances as the strong solar wind pressure compresses the magnetotail. Figure 6 shows this compression process. It displays the noon-midnight meridian of key magnetospheric properties in a similar format as Figure 4. The five rows are single instances from 22:30 to 23:10 UT, 10 minutes apart. The dynamic pressure (P_{dy}), X_{gse} component of plasma velocity (V_x), and X_{gse} component of magnetic field (B_x) are plotted in columns from left to right.

Figure 6.a and 6.b show the magnetosphere before and after the P_{sw} enhancement. At 22:30 UT before the pressure impact, the nightside magnetosphere was quiet without fast plasma flows. As the strong pressure compressed the near-Earth magnetotail at 22:40 UT, the magnetic field B_x increased in opposite directions near the central plasma sheet, initiating anti-parallel reconnection near X_{gse}= -30 Re with fast earthward plasma flows. Figure 6.c, 6.d, and 6.e show compression of the distant magnetotail. At 22:50 and 23:00 UT, the velocity of the earthward plasma flows reduced slightly from 630 km/s to ~500 km/s, and became more distributed along the length of the tail, indicating nightside reconnection activity occurring along a significant region of the tail between -30 and -80 R_E. The pressure front continued propagating downtail to a further distant tail region, compressing the whole length of the magnetotail. As a result, the magnetic field B_x increased from the near-Earth region to the very distant magnetotail, generating intense magnetic reconnection at 23:10 UT, evidenced by the strong Earthward flows in that instance. Thus, the P_{sw} enhancement of this event compressed the magnetotail strong enough to create two peaks of the nightside reconnection rate.

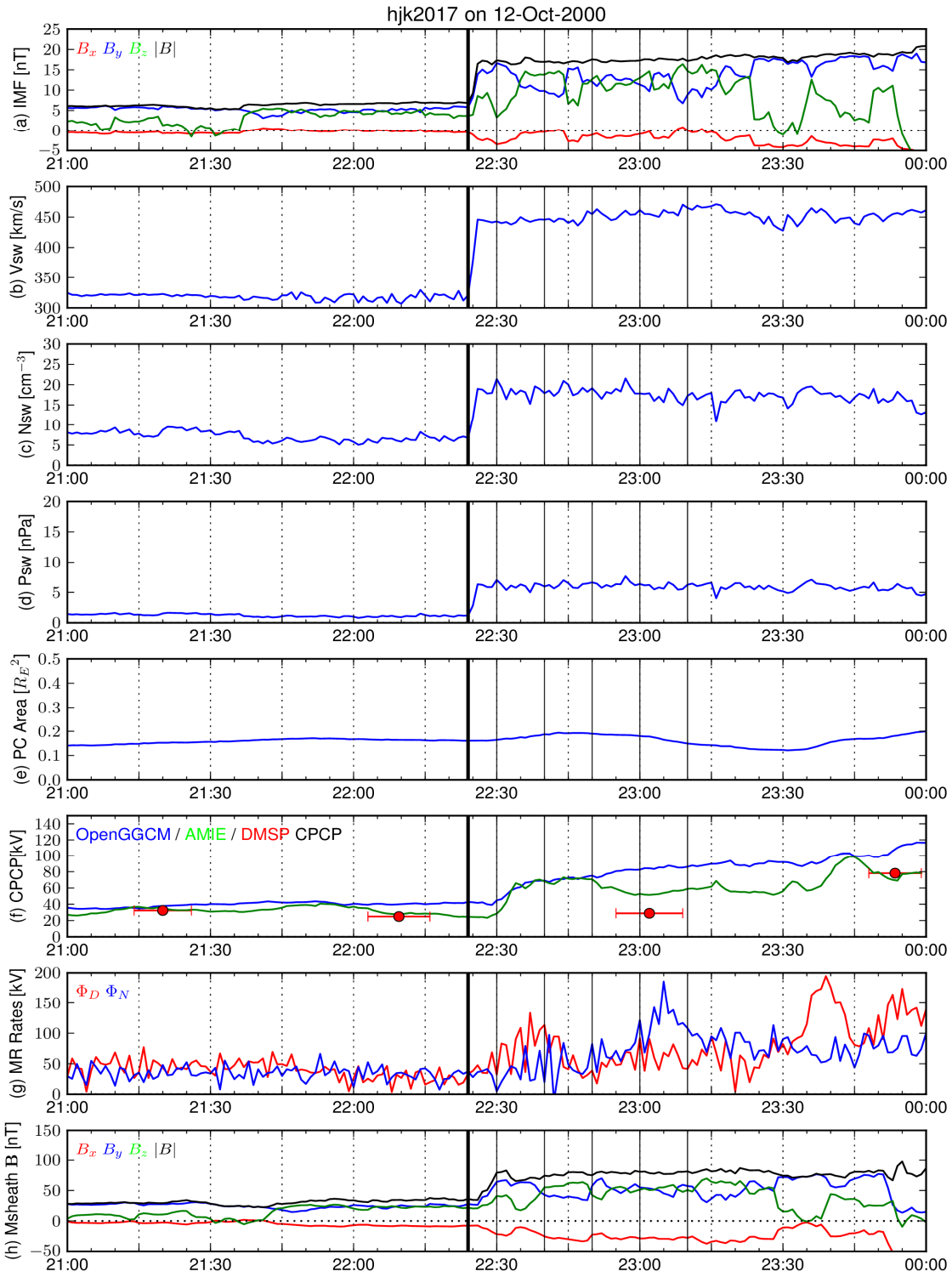

Figure 5. The Geotail spacecraft measurements of solar wind conditions (a-d) and the OpenGGCM-CTIM model results (e-h) on October 12, 2000. *See descriptions of Figure 1 for more details.*

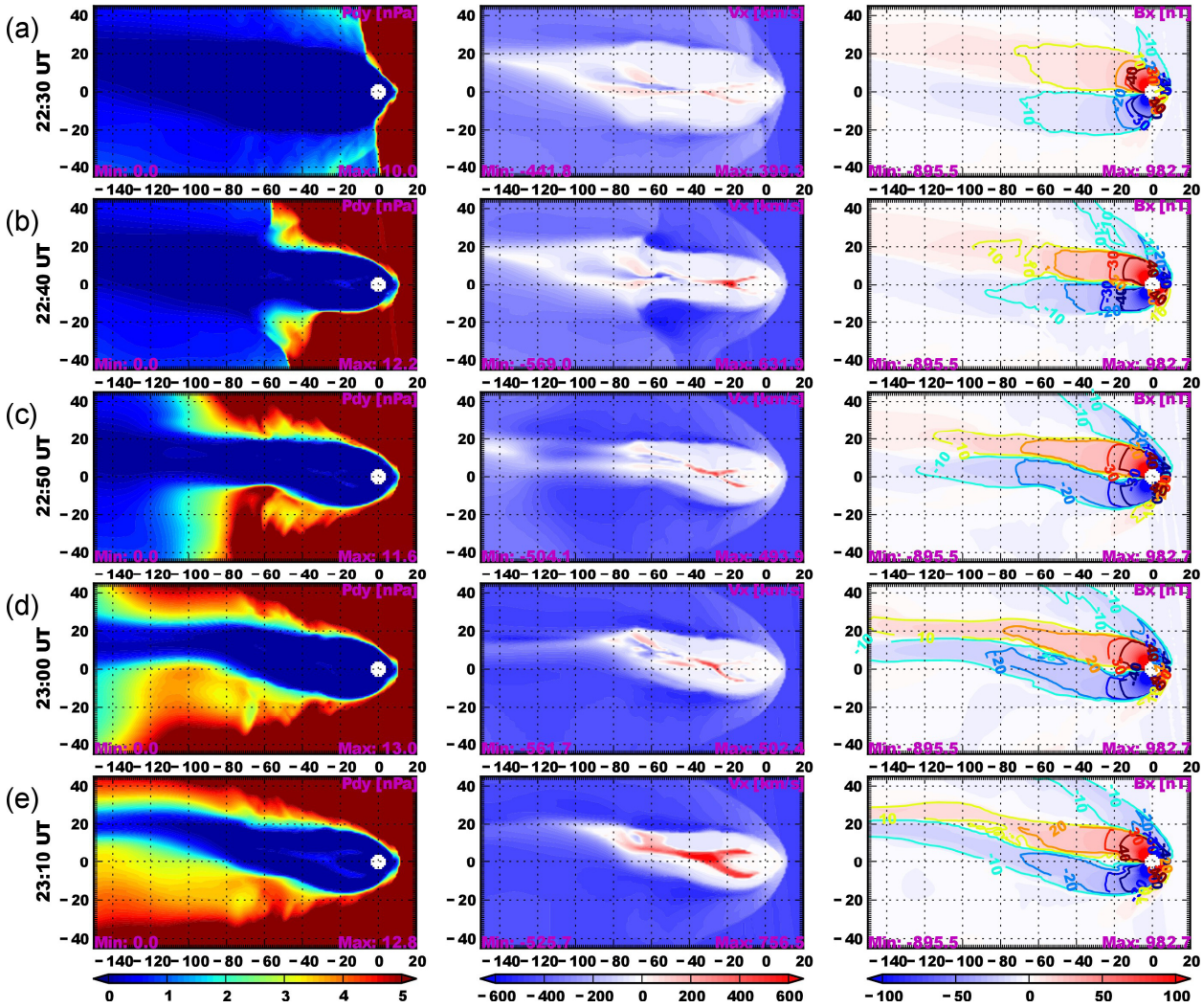

Figure 6. The OpenGGCM-CTIM magnetosphere plots during 22:30 – 23:10 UT on October 12, 2000. *Each column shows from left to right the dynamic pressure (P_{dy}), X_{gse} component of plasma velocity (V_x), and X_{gse} component of magnetic fields (B_x) on the noon-midnight meridian plane. The times of each magnetosphere plot are marked as thin vertical black lines in Figure 5.*

4. DISCUSSION AND CONCLUSION

4.1. The reconnection patterns during the sudden P_{sw} enhancement

Reconnection rates are difficult to estimate solely with observation because, to calculate the merging rates, one needs to know the motion of open-closed field line boundary across all MLT and the electric field potential patterns over the entire ionosphere. Previous studies of the merging rates [Blanchard et al., 1996, 1997; Østgaard et al., 2005; Hubert et al., 2006a] have estimated the OCB motions from 6300 Å auroral emission measurements and IMAGE FUV

images, and the ionosphere electric potentials from Sondrestrom, EISCAT, and SuperDARN radar measurements. However, ground and space observations do not provide a complete coverage of the ionosphere, and therefore the global merging patterns are difficult to obtain on a single case basis (only empirical patterns can be reliably assembled). Under such conditions, three-dimensional global magnetosphere–ionosphere–thermosphere modeling can complement the observations.

In this work three events of sudden P_{sw} enhancements using OpenGGCM-CTIM were simulated, and compared the results with DMSP, AMIE, and SuperDARN measurements. Our model produced, to a reasonable extent, the observed magnetosphere-ionosphere responses, especially the transpolar potential enhancement. The modeled CPCP showed generally good agreement with the DMSP observations and AMIE predictions.

The results obtained from our model showed that the dayside reconnection rate increases ~2 minutes after the P_{sw} enhancements and reaches its maximum within 9 – 12 minutes after the P_{sw} impact. Note that our reconnection rate is calculated based on the ionospheric values. Considering that a typical Alfven wave transit time between the magnetosphere and the ionosphere is ~2 minutes, reconnection at the dayside magnetopause intensifies immediately following the arrival of P_{sw} enhancements. The nightside reconnection rate reacts later than the dayside rate, and takes 13 – 25 minutes to reach its maximum after the pressure change. The response time scales generally match the timing of observed ionospheric convection enhancements. The SuperDARN radar observations [Boudouridis et al., 2011] have shown a dramatic increase of dayside ionospheric flows within 10 minutes of pressure impact and nightside flow enhancements in 15 – 20 minutes after the impact, in agreement with our results of the response of the dayside and nightside reconnection rates.

The dayside reconnection rate increases due to magnetosheath compression during strong solar wind pressure. This compression strengthens magnetic fields in the magnetosheath, intensifying anti-parallel reconnection on the dayside magnetopause, as predicted by theoretical merging models [Parker, 1973; Sonnerup, 1988; Dorelli et al., 2004]. The first event on Jan 10, 1997 clearly shows this process. However, in the last two events on Apr 30, 1998 and Oct 12, 2000, it was difficult to isolate this effect because the solar wind pressure enhancements were accompanied by an increase of total IMF magnitude, which in itself had the same effect on dayside reconnection rate.

The nightside reconnection rate intensified when strong solar wind pressure compressed the magnetotail. The B_x intensified in the northern and southern lobes due to this compression, intensifying anti-parallel reconnection near the central plasma sheet. All three event studies showed the enhancement of nightside reconnection rate due to the magnetotail compression. After the compression front moved into the distant magnetotail, the nightside magnetosphere behaved differently at each case, depending on whether the whole magnetosphere remained engulfed in the region of high pressure (step increase) or not (pulse increase), and on the concurrent IMF orientation.

On Jan 10 1997, the compression was a pulse and P_{sw} decreased after the initial increase to almost pre-increase levels, followed shortly afterwards by a smaller increase. The magnetotail experienced both of these successive compressions and the nightside reconnection rate increases after each compression and proportionally to the strength of each compression, all of that occurring under strong southward IMF. On Apr 30 1998, the compression was a step increase with the pressure remaining at high levels for many hours under very weak southward or near-zero IMF. Under such conditions, the nightside magnetosphere repeats the loading-unloading process as the enhanced dayside reconnection continuously loads the solar wind plasma into the magnetotail lobes. On Oct 12 2000, the P_{sw} enhancement was also a step increase lasting for many hours under northward IMF. In this case the whole magnetotail gets compressed down to the more distant magnetotail, dramatically increasing the nightside reconnection rate.

4.2. The relation between reconnection rates and the transpolar potential

To understand the relative importance of dayside and nightside reconnection on the CPCP enhancement, we used the previously defined CPCP function of the Expanding and Contracting Polar Cap (ECPC) model. This model introduces CPCP (Φ_{CPCP}) as a function of dayside and nightside reconnection rates (Φ_D and Φ_N) by assuming that the electric voltages across the dayside and nightside reconnection lines are distributed along the open-closed field line boundaries [Lockwood, 1991]. Later, the model added the viscosity effect (Φ_V), to get the equation $\Phi_{CPCP}=C_D\Phi_D+C_N\Phi_N+\Phi_V$ where the C_D and C_N are regression coefficients of the dayside and nightside reconnection rates [Lockwood and Cowley, 1992]. The regression coefficients can be considered to be a weighting factor that quantifies the contribution of each merging rate on the transpolar potential [Lockwood et al., 2009]. Here, we

linear regression method to estimate the regression coefficients and determine which reconnection dominates the CPCP, based on the above equation.

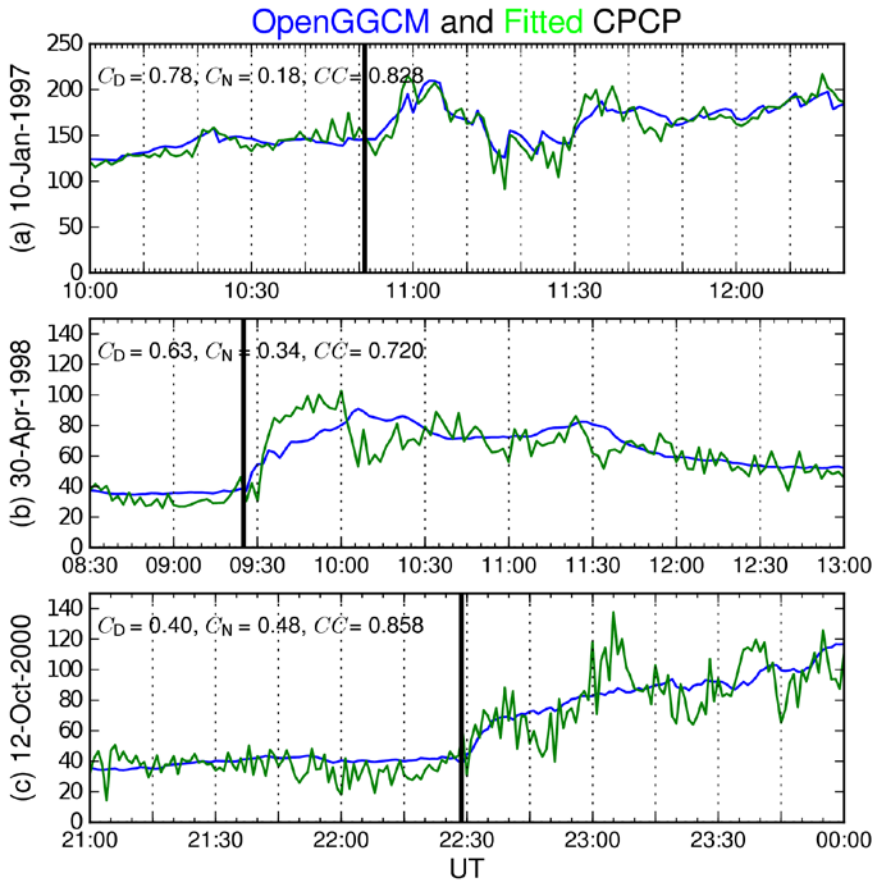

Figure 7. The CPCP fitting results of all three events. *The blue and green lines are the transpolar potentials obtained from the OpenGGCM-CTIM and the multiple linear regression analysis, respectively. The upper right corner of each panel displays the regression coefficients (C_d and C_n) and the correlation coefficient (CC) between the modeled and fitted CPCPs.*

One may question whether the regression coefficients explain a cause-effect relationship between reconnection and CPCP because, if an equation is given, the multiple linear regression method only provides correlation between any parameters regardless of their actual physical relationship. However, dayside and nightside reconnection rates have been described as CPCP contributors in previous publications [for example, Reiff et al., 1981; Boyle et al., 1997; Bristow et al., 2004; Milan, 2004a; Milan et al., 2007; Lockwood et al., 2009]. Several experiments using the ECPC model [Milan, 2004a; Lockwood et al., 2009; Gordeev et al., 2011] have demonstrated

that its CPCP equation given above follows the general behavior of the transpolar potential better than a CPCP equation without the nightside reconnection or viscosity term. Thus, there is good literature support to the equation used in this work and to the idea that both reconnection rates contribute to the CPCP and ionospheric convection on the whole. With this knowledge, the application of regression coefficients as contribution factors is a reasonable first step to understand the MI coupling dynamics. This work determined which type of reconnection controls the CPCP based on the regression coefficients. The important caveat is that no prior work has checked the accuracy of the assumed linear relationship between CPCP and the reconnection rates. It is possible, and likely during dynamic transition of the magnetosphere such as compressions, that the contribution of the reconnection rates to CPCP is not linear, but this is subject for future work. Here, the focus was on the first order relationship and it was shown that the results were physically realistic.

Next, the results were fitted to $\Phi_{CPCP} = C_D \Phi_D + C_N \Phi_N + \Phi_V$ using a multiple linear regression method, and obtained the regression coefficients which gave the best-fit results. Figure 7 shows the fitting results (green lines) as well as the original transpolar potentials obtained from the OpenGGCM-CTIM model (blue lines), for the Jan 10, 1997, Apr 30, 1998, and Oct 12, 2000 events from top to bottom, respectively. The black vertical lines indicate the pressure front impact on the dayside magnetopause for each event. In each panel, the regression coefficients (C_D and C_N) and the correlation coefficient (CC) between the modeled and fitted CPCPs are shown on the upper left corner for that event. The CC values of three events are 0.828, 0.720, and 0.858, indicating that the CPCP fit function we used provides a realistic representation of the CPCP behavior in the OpenGGCM-CTIM results.

The first solar wind pressure enhancement event occurred on January 10, 1997 during strongly southward IMF. The dayside reconnection coefficient (C_D) was 0.78, about four times stronger than the nightside coefficient (C_N). The second event happened on April 30, 1998 while IMF B_z fluctuated around zero, but for the first two hours of the pressure increase, IMF B_z was mostly weakly southward. For this event, the dayside coefficient was about two times higher than the nightside coefficient. These two event studied indicate that dayside reconnection contributes to the CPCP more significantly than nightside reconnection when solar wind pressure enhancement is accompanied by southward IMF. On the other hand, the last event on October 12, 2000 showed a higher nightside regression coefficient, suggesting that the magnetotail

reconnection has relatively stronger influence on the CPCP enhancement during northward IMF.

The physical relationship between the CPCP and the reconnection rates under the different IMF conditions were investigated by plotting the ionosphere convection patterns before and after the P_{sw} impact in the left and right columns of Figure 8 for each of the three events. The color contours, arrows, and thick black lines represent electric potentials, plasma flow vectors, and the model determined OCB of the northern ionosphere, respectively. All three events are displayed from top to bottom in Figure 8, showing that ionospheric potentials and plasma flow speeds intensify after solar wind dynamic pressure increases.

Two cell convection patterns were observed for the first two events, as expected from their southward IMF conditions (see the first two columns of Figure 8). When the P_{sw} enhancement intensified the dayside reconnection rate, strong anti-sunward plasma flows across the polar cap region were observed. The enhanced ionospheric flows were aligned along a line from 14 to 02 MLT for the Jan-10-1997 event and from 12 to 20 MLT for the Apr-30-1998 event. This anti-sunward plasma convection enhancement and the Earth's dipole magnetic field create the dawn-to-dusk electric fields, which intensifies the typical ionosphere electric field and in turn enhances the transpolar potential.

On Oct. 12, 2000, the northeast IMF condition created dayside reconnection on the high-latitude, duskside magnetopause. This reconnection produced both sunward and anti-sunward plasma flows on the dayside ionosphere. The newly-merged, kinked open field lines convected sunward due to the magnetic tension force. The ionospheric plasma was frozen-in with these field lines, producing sunward flows in the 13 – 17 MLT regions (see the bottom rows of Figure 8). These flows created the dusk-to-dawn electric fields, which oppose the typical ionospheric electric fields. As the field lines are drawn away from the reconnection sites, the magnetic tension force reduces and the magnetosheath flow moves the field lines to the anti-sunward direction. As a result, the ionospheric plasma flowed anti-sunward in 6 – 12 MLT regions, producing the dawn-to-dusk electric fields. Thus, magnetopause reconnection during northward IMF creates ionospheric convection to both increase and decrease the typical ionospheric electric fields. This weakens the contribution of dayside reconnection on the CPCP. Conversely, intense nightside reconnection during the P_{sw} enhancement produces fast anti-sunward ionospheric flows near 0 MLT, strengthening the dawn-to-dusk electric field and thus raising the transpolar potential.

This work has focused on the first-order relation between the CPCP and merging rates as a first step to understand the MI coupling dynamics during sudden enhancements of solar wind dynamic pressure. Although the ECPC model implies a linear response of CPCP to the reconnection rates, previous studies [Hill et al., 1976; Nagatsuma, 2002; Hairston et al., 2003] have demonstrated its non-linear nature by showing that, under extreme solar wind conditions, the transpolar potential no longer linearly increases with solar wind driving, but saturates instead. However, Boudouridis et al. [2004a] have shown that the Hill-Siscoe saturation model [Siscoe et al., 2002] underestimates the transpolar potential for both before and after a sudden P_{sw} enhancement. Thus, modification of existing models is necessary to fill the gap between model and observation. For future work, one must explore the complex behavior of MI dynamics by identifying the parameters responsible for the non-linear activities and developing the CPCP equation as a function of these parameters.

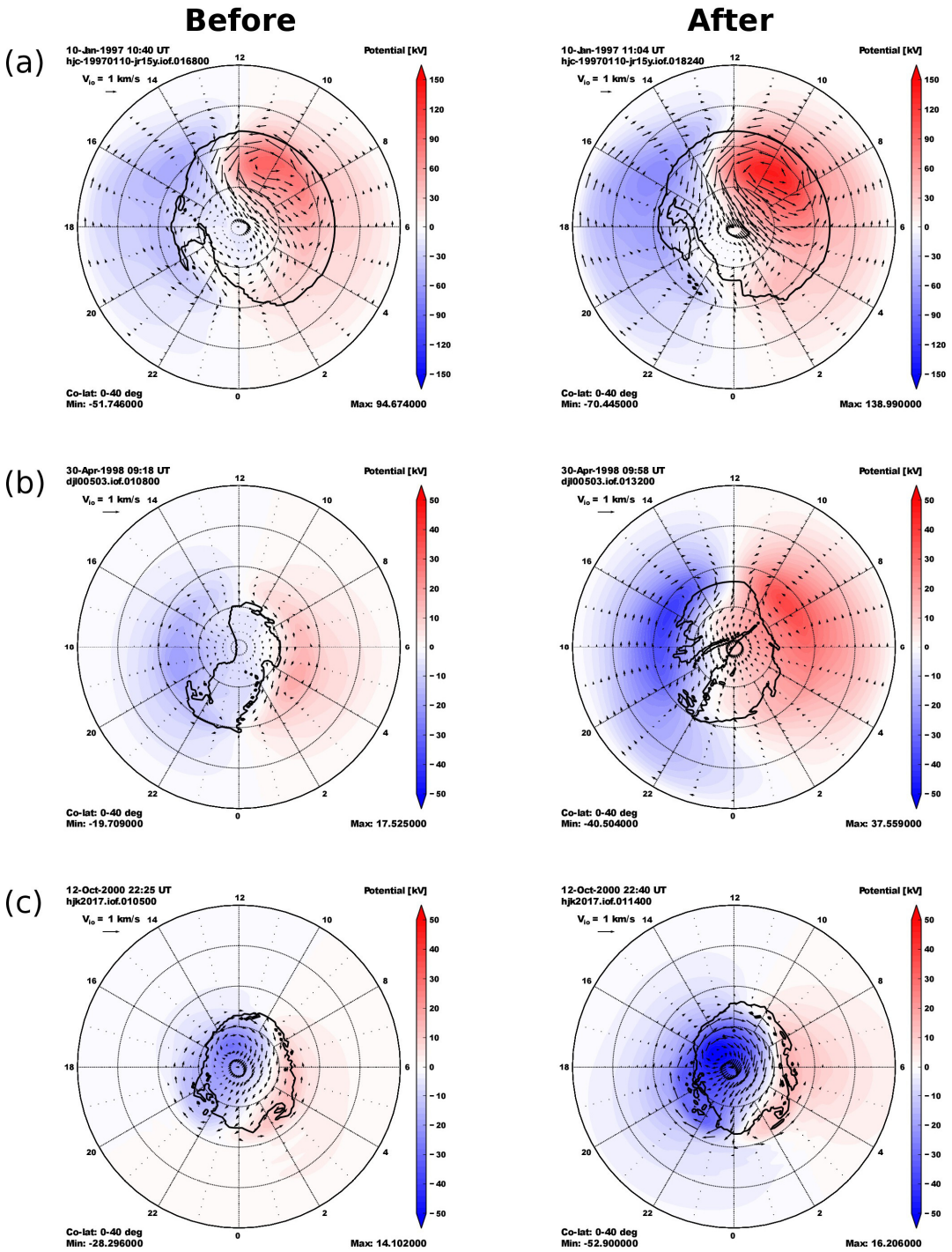

Figure 8. The OpenGGCM-CTIM ionosphere plots before and after the P_{SW} enhancements. *The top-to-bottom rows show the ionospheric conditions on January 10, 1997; April 30 1998; and October 20, 2000, respectively. The color contour represents electric potentials of the northern ionosphere. The thick black lines and arrows represent the open closed field line boundary and the ionospheric convection vectors.*

5. SUMMARY

In this work the where, when, and how solar wind energy flows into the magnetosphere-ionosphere system during sudden enhancements of solar wind dynamic pressure were investigated. The main focus was on the behavior of dayside and nightside reconnection as well as their relative importance on ionospheric convection enhancements by using CPCP as a proxy of the ionospheric convection. A detailed model analysis showed that:

1. Dayside reconnection reacts directly to P_{sw} enhancements and reaches its maximum rate within 9 – 12 minutes of the pressure impact. The event study on Jan. 10, 1997 showed that the total magnetosheath field intensifies when the strong P_{sw} compresses the magnetosheath. This initiates stronger anti-parallel reconnection on the dayside magnetopause.

2. Nightside reconnection rate reaches its maximum about 13 – 25 minutes after the pressure increase. The strong P_{sw} front compresses the magnetotail and increases magnetic field B_x near the central plasma sheet in opposite directions. This intensifies the magnetotail reconnection.

3. For southward IMF, dayside reconnection contributes to CPCP enhancement 2 – 4 times more than nightside reconnection. On the other hand, for northward IMF, dayside contribution weakens and nightside reconnection has more influence on the CPCP. High-latitude reconnection on the dayside magnetopause under northward IMF produces sunward ionospheric flows, creating a dusk-to-dawn electric field opposing and weakening the typical dawn-to-dusk convection electric field applied to the ionosphere. This leads to a weaker dayside contribution during northward IMF.

References

Blanchard, G. T., L. R. Lyons, O. de La Beaujadiere, R. A. Doe, and M. Mendillo (1996), Measurements of the magnetotail reconnection rate, J. Geophys. Res., 101, 15,265.

Blanchard, G. T., L. R. Lyons, J. T. Samson (1997), Accuracy of using the 6300 Å auroral emission to identify the magnetic separatrix on the nightside of the Earth, J. Geophys. Res., 102, 9697.

Boudouridis, A., E. Zesta, L. R. Lyons, P. C. Anderson, and D. Lummerzheim (2003), Effect of solar wind pressure pulses on the size and strength of the auroral oval, J. Geophys. Res., 108(A4), 8012, doi:10.1029/2002JA009373.

Boudouridis, A., E. Zesta, L. R. Lyons, and P. C. Anderson (2004a), Evaluation of the Hill-Siscoe transpolar potential saturation model during a solar wind dynamic pressure pulse, Geophys. Res. Lett., 31, L23802, doi:10.1029/2004GL021252.

Boudouridis, A., E. Zesta, L. R. Lyons, P. C. Anderson, and D. Lummerzheim (2004b), Magnetospheric reconnection driven by solar wind pressure fronts, Ann. Geophys., 22, pp. 1367-1378.

Boudouridis, A., E. Zesta, L. R. Lyons, P. C. Anderson, and D. Lummerzheim (2005), Enhanced solar wind geoeffectiveness after a sudden increase in dynamic pressure during southward IMF orientation, J. Geophys. Res., 110, A05214, doi:10.1029/2004JA010704.

Boudouridis, A., L. R. Lyons, E. Zesta, and J. M. Ruohoniemi (2007), Dayside reconnection enhancement resulting from a solar wind dynamic pressure increase, J. Geophys. Res., 112, A06201, doi:10.1029/2006JA012141.

Boudouridis, A., L. R. Lyons, E. Zesta, J. M. Ruohoniemi, and D. Lummerzheim (2008a), Nightside flow enhancement associated with solar wind dynamic pressure driven reconnection, J. Geophys. Res., 113, A12211, doi:10.1029/2008JA013489.

Boudouridis, A., E. Zesta, L. R. Lyons, P. C. Anderson, and A. J. Ridley (2008b), Temporal evolution of the transpolar potential after a sharp enhancement in solar wind dynamic pressure, Geophys. Res. Lett., 35, L02101, doi:10.1029/2007GL031766.

Boudouridis, A., L. R. Lyons, E. Zesta, J. M. Weygand, A. J. Ribeiro, and J. M. Ruohoniemi (2011), Statistical study of the effect of solar wind dynamic pressure fronts on the dayside and nightside ionospheric convection, J. Geophys. Res., 116, A10233, doi:10.1029/2011JA016582.

Boyle, C., P. H. Reiff, and M. Hairston (1997), Empirical polar cap potentials, J. Geophys. Res., 102(A1), pp. 111– 126.

Bristow, W. A., et al. (2004), On the observed variability of the cross-polar cap potential, J. Geophys. Res., 109, A02203, doi:10.1029/2003JA010206.

de La Beaujardiere, O., L. R. Lyons, and E. Friis-Christensen (1991), Sondrestrom radar measurements of the reconnection electric field, J. Geophys. Res., 96, 13,907.

Dorelli, J. C., M. Hesse, M. M. Kuznetsova, L. Rastaetter, and J. Raeder (2004), A new look at driven magnetic reconnection at the terrestrial solar magnetopause, J. Geophys. Res., 109.

Fuller-Rowell, T. J., D. Rees, S. Quegan, R. J. Moffett, M. V. Codrescu, and G. H. Millward (1996), A coupled thermosphere - ionosphere model (CTIM), in STEP Report, edited by R. W. Schunk, p. 217, NOAA/NGDC, Boulder, Colorado, Scientific Committee on Solar Terrestrial Physics (SCOSTEP).

Gordeev, E. I., V. A. Sergeev, T. I. Pulkkinen, and M. Palmroth, Contribution of magnetotail reconnection to the cross-polar cap electric potential drop, Journal of Geophysical Research: Space Physics (1978-2012) 116, no. A8 (2011).

Hairston, M. R., T. W. Hill, and R. A. Heelis (2003), Observed saturation of the ionospheric polar cap potential during the 31 March 2001 storm, Geophys. Res. Lett. 30(6), 1325, doi:10.1029/2002GL015894

Hill, T. W., A. J. Dessler, and R. A. Wolf (1976), Mercury and Mars: The role of ionospheric conductivity in the acceleration of magnetospheric particles, Geophys. Res. Lett., 3, pp. 429-432.

Hubert, B., S. E. Milan, A. Grocott, C. Blockx, S. W. H. Cowley, and J.-C. Gerard (2006a), Dayside and nightside reconnection rates inferred from IMAGE FUV and Super Dul Auroral Radar Network data, J. Geophys. Res., 111, A03217, doi:10.1029/2005JA011140.

Hubert, B., M. Palmroth, T. V. Laitinen, P. Janhunen, S. E. Milan, A. Grocott, S. W. H. Cowley, T. Pulkkinen, and J.-C. G´erard (2006b), Compression of the Earth's magnetotail by interplanetary shocks directly drives transient magnetic flux closure, Geophys. Res. Lett., 33, L10105, doi:10.1029/2006GL026008.

Hubert, B., C. Blockx, S. E. Milan, and S. W. H. Cowley (2009), Statistical properties of flux closure induced by solar wind dynamic pressure fronts, J. Geophys. Res., 114, A07211, doi:10.1029/2008JA013813.

Kihn, E. A., R. Redmon, A. J. Ridley, and M. R. Hairston (2006), A statistical comparison of the AMIE derived and DMSPSSIES observed high-latitude ionospheric electric field, J. Geophys. Res., Space Physics (1978-2012) 111, no. A8(2006).

Knipp, D. J. and B. A. Emery (1997), Mapping ionospheric substorm response, Adv. Space Res., 20, No 4/5, pp. 895-905.

Lockwood, M. (1991), On flow reversal boundaries and transpolar voltage in average models of high latitude convection, Planet. Space Sci., 39, pp. 397-409.

Lockwood, M. and S. W. H. Cowley (1992) Ionospheric convection and the substorm cycle, in Substorms 1, Proceedings of the First International Conference on Substorms, ICS-1, edited by C. Mattock, ESASP-335, pp. 99-109, Eur. Space Agency Publ., Noordvijk, Netherlands.

Lockwood, M., M, Hairston, I. Finch, and A. Rouillard (2009), Transpolar voltage and polar cap flux during the substorm cycle and steady convection events, J. Geophys. Res., A01210, doi:10.1029/2008JA013697.

Lyons, L. R., E. Zesta, J. C. Samson, and G. D. Reeves (2000), Auroral disturbances during the January 10, 1997 magnetic storm, Geophys., Res., Lett., 27, 3237.

Milan, S. E. (2004a), Dayside and nightside contributions to the cross polar cap potential: Placing an upper limit on a viscous-like interaction, Ann. Geophys., 22(10), pp. 3771-3777.

Milan, S. E., S. W. H. Cowley, M. Lester, D. M. Wright, J. A. Slavin, M. Fillingim, C. W. Carlson, and H. J. Singer (2004b), Response of the magnetotail to changes in the open flux content of the magnetosphere, J. Geophys. Res., 109, A04220, doi:10.1029/2003JA010350.

Milan, S. E., G. Provan, and B. Hubert (2007), Magnetic flux transport in the Dungey cycle: A survey of dayside and nightside reconnection rates, J. Geophys. Res., 112, A01209, doi:10.1029/2006JA011642.

Milan, S. E., J. Hutchinson, P. D. Boakes, and B. Hubert (2009), Influences on the radius of the auroral oval, Ann. Geophys., 27, pp. 2913-2924.

Nagatsuma, T. (2002), Saturation of polar cap potential by intense solar wind electric fields, Geophys. Res. Lett., 29(10), 1422, doi:10.1029/2001GL014202.

Ober, D. M., et al. (2001), Electrodynamics of the poleward auroral border observed by Polar during a substorm on April 22, 1998, J. Geophys. Res., 106(A4), 5927.

Ober, D. M., G. R. Wilson, N. C. Maynard, W. J. Burke, and K. D. Siebert (2006), MHD simulation of the transpolar potential after a solar-wind density pulse, Geophys. Res. Lett., 33, L04106, doi:10.1029/2005GL024655.

Ober, D. M., G. R. Wilson, W. J. Burke, N. C. Maynard, and K. D. Siebert (2007), Magnetohydrodynamic simulations of transient transpolar potential responses to solar wind density changes, J. Geophys. Res., 112, A10212, doi:10.1029/2006JA012169.

Østgaard, N., J. Moen, S. B. Mende, H. U. Frey, T. J. Immel, P. Gallop, K. Oksavik, and M. Fujimoto (2005), Estimates of magnetospheric reconnection rate based on IMAGE-FUV and EISCAT measurements, Ann. Geophys., 23, 123.

Parker, E. N. (1973), Comments on the reconnection rate of magnetic fields, J. Plasma Phys., 9, pp. 49-63.

Raeder, J., J. Berchem, and M. Ashour-Abdalla (1998), GGCM Modeling of Ionospheric Convection: The GEM Grand Challenge, Journal of Geophysical Research, 103, 14787, 1998.

Raeder, J., Y. Wang, and T. Fuller-Rowell (2001), Geomagnetic Storm Simulation With a Coupled Magnetosphere-Ionosphere-Thermosphere Model, in: Space Weather: Progress and Challenges in Research and Applications, Geophysical Monograph 125, in: 377-384, editor(s): P. Song, H. J. Singer, and G. Siscoe, Publisher: AGU, Washington D.C.

Raeder, J. (2003), Global Magnetohydrodynamics – A Tutorial, in: Space Plasma Simulation, editor(s): J. Buechner, C. T. Dum, and M. Scholer, Lecture Notes in Physics, 615, Publisher: Springer Verlag, Heidelberg, ISBN 3-540-00698-2.

Raeder, J. (2005), Polar cap potential saturation during large geomagnetic storms, Adv. Space Res., 36, 1804.

Raeder, J., D. Larson, W. Li, E. L. Kepko, and T. Fuller-Rowell (2008), OpenGGCM simulations for the THEMIS mission, Space Science Reviews, 141, 535-555, doi:10.1007/s11214-0421-5.

Reiff, P. H., R. R. Spiro, and T. Hill (1981), Dependence of polar cap potential on interplanetary parameters, J. Geophys. Res., 86(A9), pp. 7639-7648.

Siscoe, G. L., G. M. Erickson, B. U. O. Sonnerup, N. C. Maynard, J. A. Schoendorf, K. D. Siebert, D. R. Weimer, W. W. White, and G. R. Wilson (2002), Hill model of transpolar potential saturation: Comparisons with MHD simulations, J. Geophys. Res., 107(A6), 1075, doi:10.1029/2001JA000109.

Slinker, S. P., J. A. Fedder, B. A. Emery, K. B. Baker, D. Lummerzheim, J. G. Lyon, and F. J. Rich (1999), Comparison of global MHD simulations with AMIE simulations for the events of May 19–20, 1996, J. Geophys. Res., 104(A12), pp. 28379-28395, doi:10.1029/1999JA900403.

Sonnerup, B. U. O. (1988), On the Theory of Steady State Reconnection, Comp. Phys. Comm., 49, 143.

Vasyliunas, V. M. (1970), Mathematical models of magnetospheric convection and its coupling to the ionosphere, in: Particles and Fields in the Magnetosphere, D. Reidel, Dordrecht, Netherlands, p. 61.

Wolf, R. A. (1975), Effects of ionospheric conductivity on convective flow of plasma in the magnetosphere, J. Geophys. Res., 75, 4677.

Wolf, R. A. (1983), The quasi-static (slow flow) region of the magnetosphere, Solar Terrestrial Physics, Editor: R. L. Carovillano, Editor: J. M. Forbes, Publisher: D. Reidel, Hingham, MA, 303.

Zesta, E., H. J. Singer, D. Lummerzheim, C. T. Russell, L. R. Lyons, and M. J. Brittnacher (2000), The effect of the January 10, 1997, pressure pulse on the magnetosphere-ionosphere current system, in Magnetospheric Current Systems, Geophys. Monogr. Ser., vol. 118, edited by S. Ohtani et al., pp. 217–226, AGU, Washington, D. C.

DISTRIBUTION LIST

DTIC/OCP
8725 John J. Kingman Rd, Suite 0944
Ft Belvoir, VA 22060-6218 1 cy

AFRL/RVIL
Kirtland AFB, NM 87117-5776 2 cys

Official Record Copy
AFRL/RVBXP/Dr. Daniel Ober 1 cy